

Lensing Effects on the Protogalaxy Candidate cB58 and their Implications for the Cosmological Constant

T.Hamana, M.Hattori¹

Astronomical Institute, Tohoku University, Sendai 980-77, Japan

H.Ebeling, J.P.Henry

Institute for Astronomy, University of Hawaii, 2680 Woodlawn Dr, Honolulu, HI 96822, USA

T.Futamase and Y.Shioya

Astronomical Institute, Tohoku University, Sendai 980-77, Japan

ABSTRACT

The amplification of the protogalaxy candidate cB58 due to gravitational lensing by the foreground cluster of galaxies MS1512.4+3647 is quantified based on recent ROSAT and ASCA X-ray observations. It is found that the amplification is at most 25 for any reasonable cosmological model with or without cosmological constant. It is also argued that the system may be used to place new constraints on the value of the cosmological constant. The gas mass fraction for this cluster is found to be about 0.2.

Subject headings: Galaxies : clustering – Cosmology : gravitational lensing – X-rays : galaxies

¹also at the Max-Planck-Institut für Extraterrestrische Physik (MPE), D-85740 Garching, Germany

1. Introduction

The detection of galaxies at their formation epoch has been a long-standing goal. Yee et al. (1996) recently reported the discovery of a protogalaxy candidate, designated cB58, at a high redshift of $z = 2.72$. Ellingson et al. (1996) concluded that the spectral energy distribution of cB58 is most consistent with a population synthesis model (Bruzual & Charlot 1993) for young age (\sim a few 10^7 yr) and reddening of $E(B - V) \sim 0.3$. The star formation rate (SFR) inferred from the system's extremely high luminosity of $M_V \sim -26$ is $4700 M_\odot \text{yr}^{-1}$ ($H_0 = 75 \text{ km s}^{-1} \text{ Mpc}^{-1}$, $q_0 = 0.1$). Such a high SFR is enough to make all the stars in a giant galaxy within a few 10^8 years. This indicates that cB58 may be the long-sought galaxy in the initial starburst phase. When corrected to zero extinction the SFR value is still as high as $400 M_\odot \text{yr}^{-1}$. These values are extremely high compared to a mean SFR of $9.3 M_\odot \text{yr}^{-1}$ for other distant galaxies (Steidel et al. 1996a) where zero extinction is assumed. The central surface brightness of cB58 is about 21 mag/arcsec^2 in the V band (Yee et al. 1996). This is about 2 mag brighter than the mean central surface brightness of high- z ($z \sim 3$) star forming galaxies but comparable to the brightest known examples (Giavalisco et al. 1996, Steidel et al. 1996b). Thus cB58 could be regarded as one of the most active star-forming galaxy known.

However, one should consider the possible effect of amplification by gravitational lensing because, in projection, cB58 lies close ($\sim 6''$) to the center of the cluster of galaxies MS1512.4+3647 which is in the foreground at $z = 0.373$. Williams and Lewis (1996) claimed that the phenomenal properties of this protogalaxy candidate are in fact due to amplification by gravitational lensing by the foreground cluster, and that the unlensed properties of the source are typical of high-redshift starforming systems. The high surface brightness of cB58 does not rule out the lensing hypothesis, since lensing conserves surface brightness, but does require that it be atypical. However, the lensing amplification is rather sensitive to the assumed cluster mass distribution model. Therefore, detailed knowledge of the cluster mass distribution is very important to quantify the impact of amplification by lensing and to judge whether the apparently huge star formation rate of cB58 is only an artefact. X-ray observations are ideal for quantifying the cluster mass distribution. Assuming hydrostatic equilib-

rium for the X-ray emitting hot gas distribution, the measurement of the temperature and density distribution of the hot intra-cluster gas give good constraints on the cluster mass distribution. Here, we reexamine the lensing amplification effect in cB58 due to the cluster MS1512.4+3647 by constraining its mass distribution using temperature data obtained from ASCA and ROSAT PSPC observations and a gas distribution determined from ROSAT HRI observations.

Finally, we argue that cB58 provides a new opportunity to place constraints on the value of the cosmological constant, primarily because there is no lensed counter image (see Fig. 2 of Yee et al., 1996).

Throughout this paper, the Hubble constant H_0 is taken to be $75h_{75} \text{ km s}^{-1} \text{ Mpc}^{-1}$.

2. X-ray results for the cluster lens

2.1. X-ray spectral analysis

ASCA observations of MS1512.4+3647 were performed in January 1995 with an effective exposure time of 19 ks. The SIS observations were performed in 2 CCD Faint Mode for high bit rate observations and 2 CCD Bright Mode for medium bit rate observations. The Faint Mode data were converted to Bright Mode using the standard FTOOLS software. Additional data reduction was done with the standard FTOOLS and XSPEC packages. Figure 1 shows the resulting X-ray spectrum of MS1512. For GIS 2 and GIS 3, source counts were extracted from a circle of 6 arcmin radius centered on the source; for the SIS, a circle of 4.3 arcmin radius centered on the source was selected. The background was taken from the blank sky observation obtained at the same detector positions. We use the summed spectra of the two GIS and the two SIS for the spectral analysis. ROSAT PSPC observations of MS1512.4+3647 were performed in August 1992 with an exposure time of 5.2 ks. The source spectrum was extracted from a 2.5 arcmin radius circle centered on the cluster after the point source about $1'$ south of the cluster had been masked out. The background was taken from a 4.16 arcmin wide annulus around the source region within which all apparent sources had been masked out. The best fitting Raymond-Smith parameters obtained in a simultaneous fit to the ASCA and ROSAT data are summarized in Table 1 together with their 68% confidence errors for one interesting parameter, where the redshift is fixed to that of MS1512.4+3647, $z = 0.37$. The best-fit value for the hydrogen column density is consistent

Fig. 1.— X-ray spectrum of MS1512.4+3647 obtained with the ASCA GIS and SIS, as well as with the ROSAT PSPC. The summed spectra of GIS 2 and 3, and SIS 0 and 1, are shown in the upper and lower panels, respectively. The pulse height spectra are re-binned so as to contain at least 40 photons for the GIS and 20 photons for the SIS spectra in each bin. At lower energies, the lower panel also shows the spectrum obtained with the ROSAT PSPC. The pulse height spectrum is re-binned such that the count rate in each bin represents a signal to noise ratio of at least 3. A Raymond-Smith model which gives the best fit for the GIS, SIS, and PSPC spectra simultaneously is superposed.

with the Galactic value of $1.4 \times 10^{20} \text{ cm}^{-2}$ of Dickey and Lockman (1990). Figure 2 shows χ^2 contours for 68%, 90% and 99% confidence for two interesting parameters, temperature and N_H . The N_H value is well constrained by the ROSAT PSPC spectrum; the main source of error in the temperature measurement are the photon statistics of the ASCA data.

2.2. X-ray spatial analysis

ROSAT HRI observations were performed in February 1995 with an exposure time of 35 ks. Figure 3 shows the X-ray image of MS1512.4+3647 in pulse height channels 1 – 7 only since there is no significant emission from MS1512.4+3647 in channels 8 – 15. The bin size is $1 \times 1 \text{ arcsec}^2$. The astrometry is based on the position of the bright star south of MS1512.4+3647. Since the X-ray source at this position is possibly double – the poor photon statistics preclude a definitive statement – the resulting astrometry solution is only known to about 2 arcsec. The image has been adaptively smoothed using a Gaussian kernel whose size is determined from the requirement that 16 photons be covered by the kernel (Ebeling et al. 1995). The resulting Gaussian widths of the kernel range from 1.9 to 17.5 arcsec. The peak of the emission is pronounced and centered on the cluster cD. The emission from the inner $30 \text{ h}_{75}^{-1} \text{ kpc}$ radius accounts for some 15 per cent of the overall cluster emission. Although the very core region within the inner $8''$ appears spherically symmetric, the emission soon becomes significantly elongated at sizes well resolved with the HRI. Given the resolution of the HRI, there might be an asphericity in the surface brightness even in the very central region of the cluster at the (projected) location of cB58.

The radial surface brightness profile is shown in Figure 4. The point source about $1'$ south of the cluster was again excluded. There is some evidence for excess emission in the very core of the cluster which could indicate the existence of a cooling flow. However, the radial extent of the excess emission is less than 2 arcsec which is somewhat less than the HRI resolution. Also the overall significance of the excess over a pure β model is less than 3σ . Therefore, the evidence for a cooling flow in this cluster is marginal. We have fit a β model to the azimuthally averaged radial surface brightness $I(\theta)$. This model assumes

$$I(\theta) = I_0 \left[1 + \left(\frac{\theta}{\theta_c} \right)^2 \right]^{-3\beta+1/2}. \quad (1)$$

Table 1: X-ray properties of MS1512.4+3647 from the spectral analysis of ASCA/ROSAT data.

$k_b T_X$ (keV)	L_X (2 – 10 keV) ($10^{44} \text{ h}_{75}^{-2} \text{ erg s}^{-1}$)	Z_{Fe} (Z_{\odot})	N_{H} (10^{20} cm^{-2})	$\chi^2/\text{d.o.f.}$
$3.9^{+0.5}_{-0.3}$	$1.7^{+0.1}_{-0.1}$	$0.4^{+0.2}_{-0.2}$	$1.5^{+0.3}_{-0.3}$	101.4/110=0.92

The best fit parameters for this model and their 68% errors for one interesting parameter are summarized in Table 2; the resulting fit is plotted in Figure 4. The best fitting values are insensitive to whether the very central region is included in the fit or not.

According to PIMMS, an HRI count rate of 1 count s^{-1} corresponds to a flux in the 0.1 to 2.0 keV band of $3.07 \times 10^{-11} \text{ erg cm}^{-2} \text{ s}^{-1}$ for a Raymond-Smith spectrum with a temperature of 3.4 keV absorbed by a column density of $1.4 \times 10^{20} \text{ cm}^{-2}$. Using equation (5) of Henry, Briel, and Nulsen (1993) (note that there is an error in the exponent of the initial constant which should be +12 and not –12), we find the central electron density to be $n_e(0) = (0.0478 \pm 0.0066) \text{ h}_{75}^{1/2} \text{ cm}^{-3}$.

3. Constraints on the lensing amplification

We are now ready to examine the lensing amplification effects on cB58 due to the cluster of galaxies MS1512.4+3647. Our fundamental assumptions for the construction of a model of the cluster mass distribution are: (1) the X-ray emitting hot gas is in hydrostatic equilibrium with the cluster’s gravitational field, (2) the cluster has a spherically symmetric mass distribution, (3) the X-ray gas is isothermal and is in a single phase, (4) the center of the mass distribution of the cluster coincides with the center of the cD. The first of these assumptions is supported by the ratio of specific energy in galaxies and gas. Using the cluster’s galaxy velocity dispersion of $\sigma = (690 \pm 96) \text{ km s}^{-1}$ (Carlberg et al., 1996), we find this ratio, conventionally denoted by β_{spec} , to be 0.78 ± 0.23 , i.e. consistent with unity. The ratio is somewhat larger than β determined by X-ray surface brightness distribution. However Bahcall & Lubin (1994) have pointed out that the standard hydrostatic-isothermal model predicts $\beta_{\text{spec}} = (1.25 \pm 0.1)\beta$, rather than $\beta_{\text{spec}} = \beta$. Taking this into account, β_{spec} is consistent with β . The fourth assumption is true based on the HRI astrometry. Since, with ROSAT, the conversion from flux to count rate is almost constant for hot gas in the temperature range from 2 to 10 keV, and the temperature of MS1512.4+3647 in the cluster rest frame is

much higher than 2 keV, the gas density profile can be unambiguously obtained from the X-ray surface brightness profile without knowing the precise temperature distribution. According to the β model, the electron density distribution of MS1512.4+3647 is described by

$$n_e(r) = n_e(0) \left[1 + \left(\frac{r}{r_c} \right)^2 \right]^{-3\beta/2} \quad (2)$$

where $r_c = \theta_c D_{OL}$ and D_{OL} is the angular diameter distance between observer and lensing cluster. In this equation, as in the following, r_c/D_{OL} and β are taken to be 6.90 ± 1.37 arcsec and 0.524 ± 0.031 , respectively.

Inverting the hydrostatic equilibrium equation yields the cluster mass contained within a radius r :

$$M(r) = \frac{kT}{G\mu m_{\text{H}}} 3\beta \frac{r^3}{r_c^2} \frac{1}{1 + (r/r_c)^2} \quad (3)$$

where $\mu = 1.3/2.1$ is the mean molecular weight for gas of cosmic abundance. The lens equation for this mass distribution is

$$\tilde{\theta}_S = \tilde{\theta}_I - D \frac{\tilde{\theta}_I}{\sqrt{\tilde{\theta}_I^2 + 1}} \quad (4)$$

where

$$D \equiv \frac{6\pi\beta}{\theta_c} \frac{kT}{\mu m_{\text{H}} c^2} \frac{D_{LS}}{D_{OS}}, \quad (5)$$

θ_c is the angular core radius, $\tilde{\theta}_S$ ($\tilde{\theta}_I$) is the angle between the lens and the source (image) in units of θ_c , and D_{LS} (D_{OS}) is the angular diameter distance between the lens (the observer) and the source (the explicit expression is given in Fukugita et al. 1992). D is called the lens parameter and determines the efficiency of the lens. It should be noted that, as the lens parameter does not depend on the Hubble constant, neither do the amplification effects on cB58. When $D \leq 1$, the lens always produces a single image. On the other hand, when $D > 1$, a counter image may be produced if $\tilde{\theta}_S$ is sufficiently small to satisfy the condition

$$|\tilde{\theta}_S| < (D^{2/3} - 1)^{\frac{3}{2}}, \quad \text{for } D > 1. \quad (6)$$

Table 2: X-ray properties of MS1512.4+3647 from the spatial analysis of ROSAT HRI data.

I_0 (count s ⁻¹ arcsec ⁻²)	θ_c arcsec	β	$\chi^2/\text{d.o.f.}$
$(2.34 \pm 0.42) \times 10^{-5}$	6.90 ± 1.37	0.524 ± 0.031	7.91/8 = 0.99
$(2.15 \pm 0.40) \times 10^{-5}$	7.48 ± 1.54	0.533 ± 0.034	5.52/6 = 0.92

Fig. 4.— Radial surface brightness profile of MS1512.4+3647 obtained from ROSAT HRI observations. The best-fitting β model for all radial bins is superposed in the left panel. The best-fitting β model for all radial bins except for the central two is superposed in the right panel.

The lens parameter for cB58 is $D \sim 1.4$ for $\beta = 0.52$, $k_b T = 3.9$ keV, and $\theta_c = 6''.9$ in an Einstein-de Sitter universe, i.e. $(\Omega_0, \lambda_0) = (1, 0)$ with Ω_0 being the density parameter and λ_0 the normalized cosmological constant. In the following, we shall mainly consider the following three extreme models; spatially flat universes with $(\Omega_0, \lambda_0) = (1, 0)$ and $(0.1, 0.9)$ and the open universe with $(\Omega_0, \lambda_0) = (0.1, 0)$.

Yee et al. (1996) observed cB58 with the Canada-France-Hawaii Telescope. The seeing was $0''.64$ and $0''.73$ FWHM for the averaged I and V bands respectively. With a width of $\sim 2''$ (sufficiently larger than the seeing) the image of cB58 is well resolved. We approximate the observed image of cB58 as an ellipse with a semi-major axis of $1''.5$ and an axis ratio of 1.6. See Figure 6 and compare to Figure 2 of Yee et al. (1996).

Using the lens equation (4), we can create the un-lensed source image by mapping the observed image back onto the source plane. The amplification is then calculated as the ratio of the areas of the observed and the un-lensed images. Figure 5 demonstrates how sensitive the amplification is to variations in the cluster core radius and temperature. The positions of

Fig. 2.— χ^2 contours for 68%, 90% and 99% confidence obtained by spectral fitting of the ASCA and ROSAT data. The plus sign marks the best fit values of column density and temperature.

Fig. 3.— Contours of the adaptively smoothed ROSAT HRI image of MS1512.4+3647 overlaid on 1800s R band exposure obtained with the University of Hawaii 88inch telescope in $0''.6$ seeing (from Gioia & Luppino 1994, image kindly made available by I. Gioia). The contours are placed at constant \log_{10} intervals with the lowest contour being 50% above the background. The spacing corresponds to an increase of 25% between adjacent contours, resulting in 14 levels from 0.13 to 2.28 in units of 10^{-5} count arcsec $^{-2}$ s $^{-1}$.

the peaks correspond to configurations where the observed image position coincides with a critical line (Schneider et al. 1992). In the region where condition (6) is satisfied a bright counter image appears. It is important to realize that the amplification may become large even in the single image case and that it is possible to have a strongly magnified lensed image without large image distortion. The general physical mechanism for forming such a lensed image is discussed by Futamase, Hamana & Hattori (1997).

Figure 6 shows the counter image (left), the unlensed source image mapped onto the lens plane (center), and the observed image (right) for various values of θ_c . In the case of Figure 6b, the observed image straddles a critical line, therefore the predicted source image consists of two parts of opposite parity. In the case of Figure 6c, there is no counter image and the predicted source image is less distorted.

The magnitude difference between the observed image and the counter image is shown in Figure 7. When the core radius is small enough for a counter image to appear, the latter must be at least as bright as the observed image. The fact that no such bright counter image is observed in the field around the cD galaxy, together with the measured temperature and mass distribution for the cluster, provides strong constraints on the amplification of the observed image.

Figure 8(a)-(c) shows the allowed region for temperature and core radius as well as lines of constant amplification for the single image situation for three cosmological models, namely $(\Omega_0, \lambda_0) = (1, 0)$, $(0.1, 0)$, and $(0.1, 0.9)$ respectively. From Figure 8(d), it can be seen that a large cosmological constant reduces the single image region drastically. The reason for this is the following: Condition (6), which determines when a counter image is produced, is expressed in terms of the lens parameter which, in turn, depends on the gas temperature, the core radius of the cluster mass distribution and a combination of two angular diameter distances. The first two quantities can be constrained by X-ray observations as shown in Section 2. The last one depends strongly on the value of the cosmological constant (Fukugita, Futamase & Kasai 1990). Therefore, the value of the cosmological constant can, in principle, be constrained by the requirement that there be no counter image of cB58. This new test was first proposed by Futamase, Hamana & Hattori (1997), and cB58 is the first and very good application of this method.

If the best fit value of the temperature from the

Fig. 5.— Amplifications for $k_b T = 3.6$ keV (solid lines), 3.9 keV (dotted lines) and 4.4 keV (dashed lines). The vertical lines mark the boundary between the multiple and single image region. In the region leftward of the line, a bright counter image appears. (a), (b) and (c) are for $(\Omega_0, \lambda_0) = (1, 0)$, $(0.1, 0)$ and $(0.1, 0.9)$ respectively.

Fig. 6.— Expected counter image (left), source (center) and observed image (right). The plots in panels (a), (b), and (c) assume $\theta_c = 5.5, 6.9,$ and 8.5 arc-sec respectively; $k_b T = 3.9$ keV and $(\Omega_0, \lambda_0) = (1, 0)$ throughout. Note that no counter image appears in the lower panel.

Fig. 7.— The difference in magnitude between the observed and the counter image, $\Delta m = m(\text{observed image}) - m(\text{counter image})$ for $k_b T = 3.9$ keV and $(\Omega_0, \lambda_0) = (1, 0)$.

Fig. 8.— Allowed regions in the $\theta_c - k_b T$ plane. The solid line marks the boundary between the multiple and single image region. A counter image is expected for $\theta_c - k_b T$ combinations that lie above and left of the solid line. Lines of constant amplification are shown dashed. The plus and dotted box denote the best fit and 68% errors of the core radius obtained from ROSAT HRI data (for all radial bins) and the X-ray temperature obtained from ASCA and ROSAT PSPC data, respectively. (a), (b) and (c) are for $(\Omega_0, \lambda_0) = (1, 0)$, $(0.1, 0)$, and $(0.1, 0.9)$ respectively. (d) The boundaries are shown for universe models with $\lambda_0 + \Omega_0 = 1$. From upper to lower $\lambda_0 = 0, 0.2, 0.4, 0.6$ and 0.8 .

ASCA and ROSAT PSPC analysis and the best fit value of the core radius from the ROSAT HRI analysis are assumed, any universe model with reasonable cosmological parameters predicts a bright counter image of cB58 which is not observed. If the 1σ errors in temperature and core radius are taken into account, both an open universe and a flat universe with zero cosmological constant are acceptable and predict that the amplification of cB58 can be as large as 25. However, only a small part of the temperature–core radius region is allowed. On the other hand, a flat universe with a large cosmological constant does not have any acceptable region.

However, if 2σ or 3σ measurement errors are taken into account, the above mentioned constraints are relaxed. The statistical errors in the temperature is large: $k_b T = 3.9_{-0.6}^{+0.9}(2\sigma)$, $_{-0.9}^{+1.5}(3\sigma)$. A flat universe with a large cosmological constant can have an acceptable region. A large range of amplifications from several to 25 is possible regardless of the cosmological models. If the lensing amplification of cB58 were 50, its intrinsic star formation rate would be reduced to a value found for other distant galaxies (Steidel et al., 1996a). Hence, although such a high amplification is improbable, we can not definitely determine whether cB58 really features a very high star formation rate or is just a normal starburst galaxy at high redshift.

How sensitive is this result to changes in our model assumptions? One of our initial assumptions was that the X-ray emitting gas is isothermal and in a single phase. If a cooling flow existed in MS1512.4+3647 it would cause the gas to be multiphase in the central region of the cluster. Allen et al. (1996) claimed that for clusters hosting strong cooling flows the use of a single phase model can lead to significant underestimates of the overall temperature. Accordingly, a strong cooling flow in MS1512.4+3647 would mean a higher lower limit to the lensing amplification and more severe constraints on the cosmological constant. However, contrary to the results from earlier work (Stoche et al, 1991), we find the evidence for a cooling flow to be marginal for this cluster.

We also assumed that the cluster has a spherically symmetric mass distribution. The ROSAT HRI image (Figure 3), however, shows the X-ray emission to be asymmetric outside of the core region. Bartelmann (1995) has pointed out that deviations from spherical symmetry in cluster lenses enhance the tidal effect (shear) and alter the lensing efficiency of the cluster. However, to allow the effects of the asym-

metry in MS1512.4+3647 to be quantified, an accurate spatial model of the mass distribution is required. Such a model is now being developed.

The observations presented here may be used to measure the gas mass fraction in this cluster. Inserting the central gas density found in Section 2.2 into equation (2) and integrating out to the maximum radius detected ($100''$ or $0.42 h_{75}^{-1}$ Mpc), we find a gas mass of $(2.14 \pm 1.74) \times 10^{13} h_{75}^{-5/2} M_{\odot}$. This mass is proportional to the core radius cubed, which accounts for the large error, see Table 2. The total mass out to the same radius, from equation (3) is $(9.20 \pm 1.09) \times 10^{13} h_{75}^{-1} M_{\odot}$. Hence the gas mass fraction is $(0.23 \pm 0.19) h_{75}^{-3/2}$. This value, although poorly constrained, is consistent with that of low redshift clusters (White and Fabian, 1995).

4. Conclusion

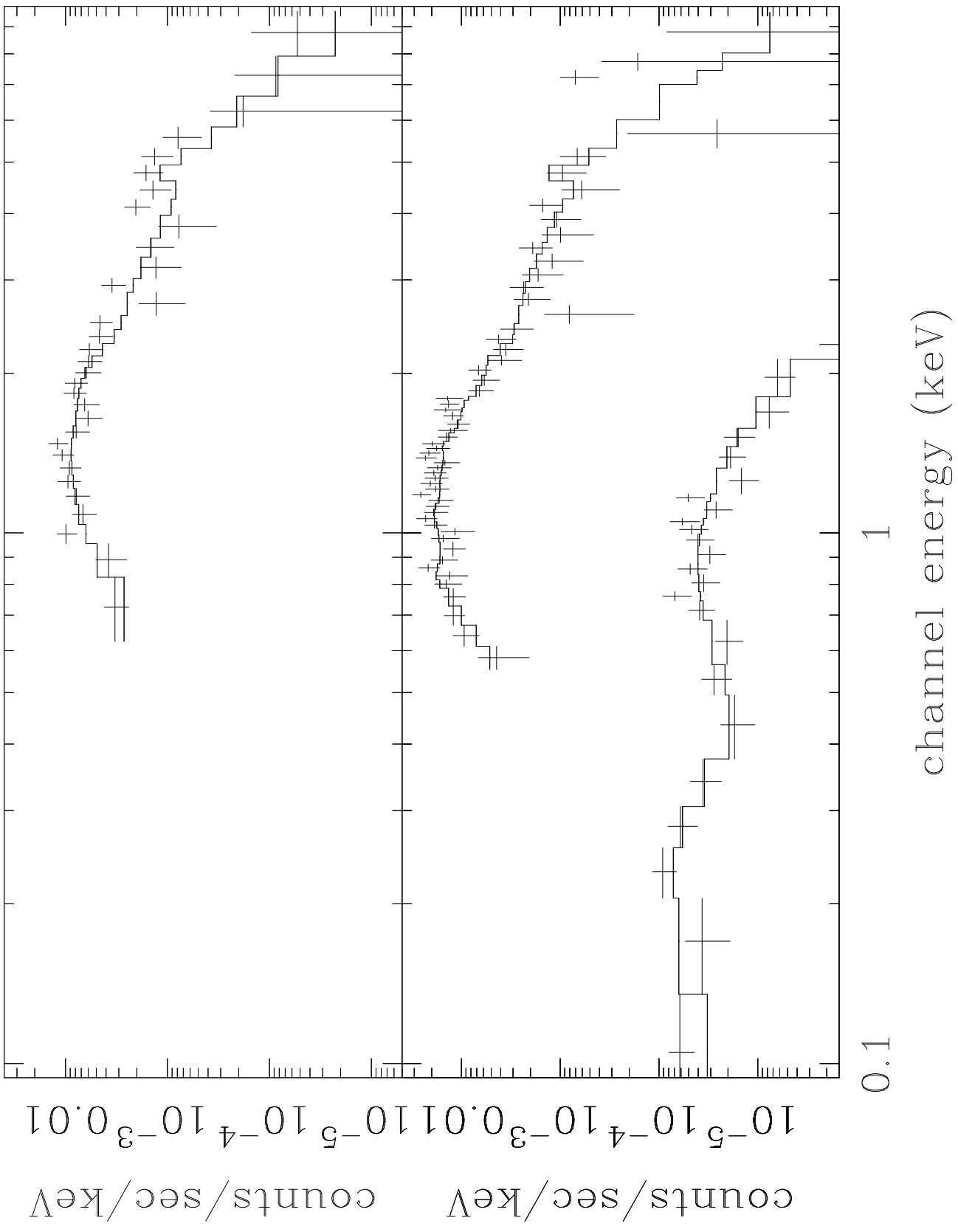
We have examined the amplification of cB58 due to gravitational lensing by the foreground cluster of galaxies MS1512.4+3647 based on ROSAT and ASCA X-ray observations of the cluster. Unfortunately, with the available X-ray observations we cannot specify the physical parameters of the foreground cluster MS1512.4+3647 accurately enough to evaluate the lensing amplification and definitely determine whether cB58 is a normal star forming galaxy. We have also shown that cB58 allows a new and promising test to constrain the value of the cosmological constant. In this study, however, we cannot give a strong constraint on the cosmological constant, because of large statistical errors in our X-ray observations. If one could measure an accurate mass distribution for MS1512.4+3647, particularly its ellipticity, then the observational fact that no counter image of cB58 is observed would give a strong constraint on the cosmological constant. From both points of view, it is highly desirable to perform further observations to obtain more accurate information on the temperature and the mass distribution of the cluster MS1512.4+3647.

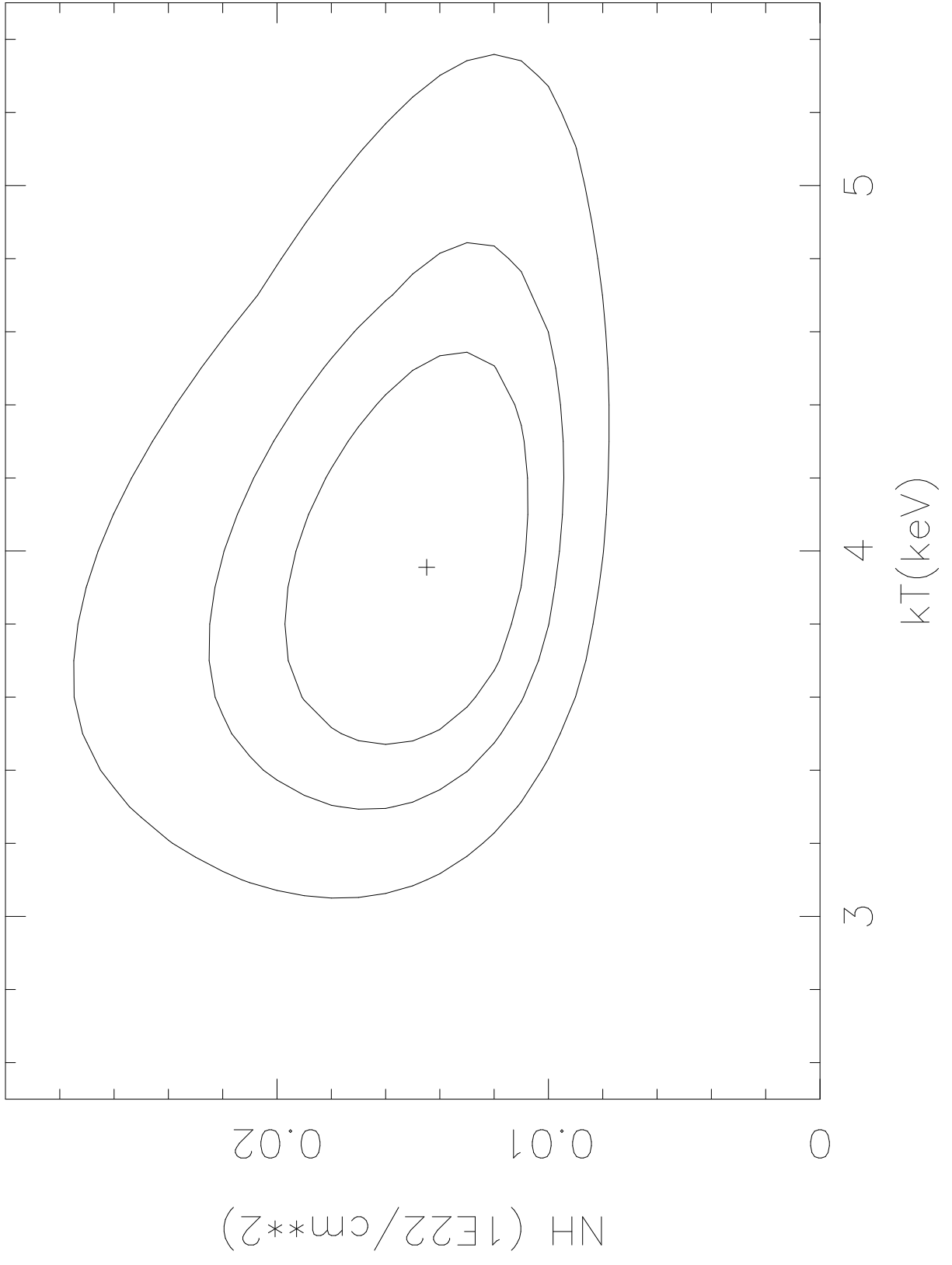
It is a pleasure to thank T. Yamada for useful discussions. We also thank I. Gioia for making available to us the optical image of MS1512.4+3647. MH thanks D. Neumann and T. Miyaji for useful comments on X-ray data analysis. MH would like to thank the Max-Planck-Institut and the Yamada Science Foundation for financial support. HE gratefully acknowledges financial support from SAO contract

SV4-64008, JPH's research has been supported by NASA grants NAG 5-1880 (ROSAT) and NAG 5-2513 (ASCA) and by NSF grant AST 95-00515. This work is supported in part by Japanese Grant-in-Aid for Science Research of Ministry of Education, Science and Culture, No. 07640366.

REFERENCES

- Allen S. W., Fabian A. C., Kneib J. P., 1996, MNRAS, **279**, 615
- Bahcall N. A., Lubin L. M., 1994, ApJ **426**, 515
- Bartelmann M., 1995, A&A **299**, 11
- Bruzual G. A., Charlot S., 1993, ApJ **405**, 538
- Carlberg R. G., Yee H. K. C., Ellingson E., Abraham R., Gravel P., Morris S., Pritchett C. J. 1996, ApJ **462**, 32
- Dickey J. M., Lockman F. J., 1990, ARA&A **219**, 18.
- Ebeling H., White D. A., Rangarajan F. V. N. 1995, MNRAS, submitted
- Ellingson E., Yee H. K., Bechtold J., Elston R. 1996, ApJ **466**, L71
- Fukugita M., Futamase T., Kasai M., 1990, MNRAS **246**, 21P
- Fukugita M., Futamase T., Kasai M., Turner E. L., 1992, ApJ **393**, 3
- Futamase T., Hamana T., Hattori, M. 1997, in preparation
- Giavalisco M., Steidel C. C., Macchetto F. D., 1996, ApJ **470**, 189
- Gioia I. M., Luppino G. A., 1994, ApJS **94**, 583
- Henry, J. P., Briel, U. G., Nulsen, P. E. J. 1993, A&A, **271**, 413
- Schneider P., Ehlers J., Falco E. E., 1992, Gravitational Lenses (Heidelberg: Springer)
- Squires G., Neumann D. M., Kaiser N., Arnaud M., Babul A., Böhringer H., Fahlman G., Woods D., 1996, ApJ, submitted.
- Steidel C. C., Giavalisco M., Pettini M., Dickinson M., Adelberger K. L., 1996a, ApJ **462**, L17
- Steidel C. C., Giavalisco M., Dickinson M., Adelberger K. L., 1996b, AJ **112**, 352
- Stocke J. T., Morris S. L., Gioia I. M., Maccacaro T., Schild R., Wolter A., Fleming T. A., Henry J. P., 1991, ApJS **76**, 813
- White, D. A. Fabian, A. C. 1995, MNRAS, **273**, 72
- Williams L. L. R., Lewis G. F. 1996, MNRAS **281**, L35
- Yee H. K. C., Ellingson E., Bechtold J., Carlberg R. G., Cuillandre, J.-C., 1996, AJ **111**, 1783





This figure "fig3.jpg" is available in "jpg" format from:

<http://arxiv.org/ps/astro-ph/9703136v1>

